BRNO UNIVERSITY OF TECHNOLOGY

Faculty of Mechanical Engineering

BACHELOR'S THESIS

Brno, 2021   Daniel Lipták

BRNO UNIVERSITY OF TECHNOLOGY

VYSOKÉ UČENÍ TECHNICKÉ V BRNĚ

FACULTY OF MECHANICAL ENGINEERING

FAKULTA STROJNÍHO INŽENÝRSTVÍ

INSTITUTE OF PHYSICAL ENGINEERING

ÚSTAV FYZIKÁLNÍHO INŽENÝRSTVÍ

NANODEVICES ON GRAPHENE PREPARED BY AFM MECHANICAL LITHOGRAPHY

NANOZAŘÍZENÍ NA GRAFENU PŘIPRAVENÁ MECHANICKOU LITOGRAFII AFM

BACHELOR'S THESIS
BAKALÁŘSKÁ PRÁCE

AUTHOR   Daniel Lipták
AUTOR PRÁCE

SUPERVISOR   Ing. Vojtěch Švarc
VEDOUCÍ PRÁCE

BRNO 2021

Assignment Bachelor's Thesis

Institut:	Institute of Physical Engineering
Student:	**Daniel Lipták**
Degree programm:	Applied Sciences in Engineering
Branch:	Physical Engineering and Nanotechnology
Supervisor:	**Ing. Vojtěch Švarc**
Academic year:	2020/21

As provided for by the Act No. 111/98 Coll. on higher education institutions and the BUT Study and Examination Regulations, the director of the Institute hereby assigns the following topic of Bachelor's Thesis:

Nanodevices on graphene prepared by AFM mechanical lithography

Brief Description:

Graphene is a monolayer of carbon atoms in a hexagonal arrangement, which has properties suitable for the production of nanoelectronic devices, e. g. the possibility of changing the type of charge carriers due to gate voltage and high mobility of charge carriers. However, in order to reduce the longitudinal dimensions of graphene, it must be patterned by a suitable lithographic technique, which would not significantly impair the mentioned electronic properties of graphene and at the same time achieve sufficiently small (nanometer) dimensions. The aim of this work is to test the possibilities of atomic force microscope (AFM) mechanical lithography in the preparation of nanodevices on graphene and to verify the insulating properties of prepared barriers by simultaneous measurement of transport response and Kelvin probe microscopy (KPFM) of functional nanodevices.

Bachelor's Thesis goals:

1. Literature research of the mentioned issue with an emphasis on the possibilities of AFM lithography of graphene.
2. Prepare the following nanostructures on graphene by AFM mechanical lithography:
a. interruption in the form of an insulating barrier
b. Narrowing in the form of a quantum point contact.
3. Characterize these devices by simultaneous mapping using:
a. transport response and
b. Kelvin probe force microscopy.

Recommended bibliography:

CASTRO NETO, A. H., F. GUINEA, N. M. R. PERES, K. S. NOVOSELOV a A. K. GEIM. The electronic properties of graphene. Reviews Of Modern Physics [online]. American Physical Society, 2009, 81(1), 109-162 [cit. 2020-10-22]. ISSN 0034-6861.

VASIĆ, Borislav, Markus KRATZER, Aleksandar MATKOVIĆ, et al. Atomic force microscopy based manipulation of graphene using dynamic plowing lithography. Nanotechnology [online]. 2013, 24(1), 015303 [cit. 2020-10-22]. ISSN 0957-4484.

KONEČNÝ, Martin, Miroslav BARTOŠÍK, Jindřich MACH, et al. Kelvin Probe Force Microscopy and Calculation of Charge Transport in a Graphene/Silicon Dioxide System at Different Relative Humidity. ACS applied materials & interfaces [online]. 2018, 10(14), 11987-11994 [cit. 2020-10-22]. ISSN 19448244.

Deadline for submission Bachelor's Thesis is given by the Schedule of the Academic year 2020/21

In Brno,

L. S.

....

prof. RNDr. Tomáš Šikola, CSc.   doc. Ing. Jaroslav Katolický, Ph.D.
Director of the Institute   FME dean

ABSTRACT

In this bachelor's thesis, we focused on the preparation of nano-structures on graphene, namely using mechanical lithography as our chosen method of graphene interruption, by an Atomic Force Microscope (AFM). Using Kelvin Probe Force Microscopy (KPFM), the insulating capabilities of prepared barriers are then verified.

ABSTRAKT

Táto bakalárska práca je zameraná na tvorbu nano-štruktúr na graféne, použitím mechanickej litografie ako spôsob prerušenia grafénu, pomocou mikroskopu atomických síl. Pomocou Kelvinovej silovej mikroskopie, izolačné schopnosti pripravených bariér sú potom potvrdzované.

KEYWORDS

AFM, mechanical lithography, graphene, KPFM

KĽÚČOVÉ SLOVÁ

AFM, mechanická litografia, grafén, KPFM

Author's Declaration

Author:	Daniel Lipták
Author's ID:	211549
Paper type:	Bachelor's Thesis
Academic year:	2020/21
Topic:	Nanodevices on graphene prepared by AFM mechanical lithography

I declare that I have written this paper independently, under the guidance of the advisor and using exclusively the technical references and other sources of information cited in the paper and listed in the comprehensive bibliography at the end of the paper.

As the author, I furthermore declare that, with respect to the creation of this paper, I have not infringed any copyright or violated anyone's personal and/or ownership rights. In this context, I am fully aware of the consequences of breaking Regulation § 11 of the Copyright Act No. 121/2000 Coll. of the Czech Republic, as amended, and of any breach of rights related to intellectual property or introduced within amendments to relevant Acts such as the Intellectual Property Act or the Criminal Code, Act No. 40/2009 Coll. of the Czech Republic, Section 2, Head VI, Part 4.

Brno . . . .　　　　　. . . . .
　　　　　　　　　　　　　　　　　　　　　　author's signature*

---

*The author signs only in the printed version.

ACKNOWLEDGEMENT

Contents

Introduction

In a world filled with desire for the new and exciting, recent technological advances have been a key ingredient in keeping our surroundings just that. However, such progress requires the study and preparation of new materials and testing them to their fullest potential.

A new field in material analysis has emerged- 2D material development. Among such nano-scale materials is graphene, an allotrope of carbon. Although, the material was not discovered until recently (2004), it propelled a wide variety of experiments and further studies of other 2D materials.

So as to explore the capabilities of graphene, we will be using a technique referred to as "mechanical lithography" using an Atomic Force Microscope (AFM) to interrupt our graphene samples.

In the first chapter of this bachelor's thesis, we introduce graphene as a nanomaterial, describe its structure, its most notable electric properties and describe a couple of methods of graphene preparation. Secondly, we will be describing AFM, the probes the microscopes use and their imaging modes. Finally, we will be describing Kelvin Probe Force Microscopy (KPFM), which we used for the measurement of the surface potential of our samples.

In the second chapter, we provide a brief literature research into similar topics and techniques, which were used either in the past or present to interrupt graphene. On the other hand, we will be touching on charge dissipation as well.

In the experimental part of the thesis, we will be going over the sample preparation process, the setup of the AFM, the preparation of our nano-structures and finally, the charging and measurement of surface potential (with the use of KPFM) on these samples.

1 Theory

1.1 Graphene

1.1.1 Basics of graphene

Carbon is an unimaginably important element in the world of organic chemistry. Life as we know it, would be impossible without its existence. Carbon has the unique ability to form long chains with itself and to bind to other elements to make ever-increasingly complex materials and chemicals in the process. It is this complexity that allows it to have greater functions, be it in molecular biology, organic chemistry and even nano-physics [1].

When we talk about materials containing only carbon atoms, graphene is a prime example. Graphene is an allotrope of carbon, which happens to be a two-dimensional sheet of atoms arranged in a honeycomb lattice. These hexagons could be interpreted as benzene rings, which are connected to one another. These benzene rings are stripped of their hydrogen atoms.

Other, lower dimensional, carbon allotropes include: carbon nanotubes and fullerenes. Carbon nanotubes are wrapped up graphene sheets, which have only one physically meaningful dimension, their length. Fullerenes are physically considered zero-dimensional, because the carbon atoms are arranged in a spherical fashion by the introduction of pentagons, which create positive curvature defects.

Graphite, a widely known allotrope of carbon, is a three-dimensional material, which is comprised of stacks of graphene layers held together by van der Waals forces. This property made it a preferred material during the creation of the pencil in the second half of the 16$^{\text{th}}$ century. The act of pressing the graphite tip of a pencil was enough to break off layers of graphene and discolor the surface of the targeted object. One could presume, that humanity has been producing prime graphene samples on paper for over four hundred years, without knowledge of doing so.

Although graphene has been around for a long time, it was only discovered recently, because of the optical effects it creates on top of silicon dioxide substrates. This subtle effect is observable with an optical microscope, allowing its direct observation.

Structural flexibility is one of the main properties of the hexagonal lattice, because of a σ bond between the carbon atoms. This is due to the sp^2 hybridization between one s and two p orbitals, leading to the trigonal planar structure and the distance between each carbon atoms is $1.42\,\text{Å}$. This structure is the cause behind the fact, that these allotropes are so robust with high structural integrity [2]. Such properties are extremely important when it comes to repositioning graphene.

1.1.2 Atomic structure of graphene

The structure can be described as a triangular lattice with a basis of two atoms per unit cell. Then the lattice vectors can be written as:

$$\vec{a}_1 = \frac{a}{2}\left(3, \sqrt{3}\right), \qquad \vec{a}_2 = \frac{a}{2}\left(3, -\sqrt{3}\right), \qquad (1.1)$$

where $a \approx 1.42\,\text{Å}$ is the distance between carbons. The reciprocal-lattice vectors are then given by:

$$\vec{b}_1 = \frac{2\pi}{3a}\left(1, \sqrt{3}\right), \qquad \vec{b}_2 = \frac{2\pi}{3a}\left(1, -\sqrt{3}\right). \qquad (1.2)$$
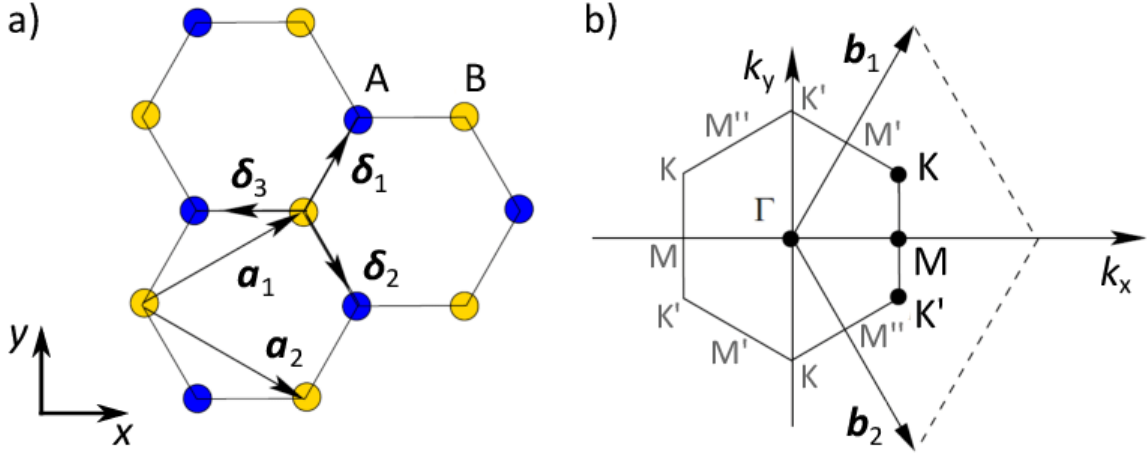

Fig. 1.1: Honeycomb lattice (a) and its Brillouin zone (b), adapted from [3].

In Fig. 1.1: (a) we can see the lattice structure of graphene, made of two interpenetrating triangular lattices (where $\vec{a}_1$ and $\vec{a}_2$ are the unit vectors and δ_i, i=1,2,3 are the nearest-neighbor vectors). In part (b) we can see the corresponding Brillouin zone. The Dirac cones are each located at the K and K' points.

The three nearest-neighbor vectors in real space are given by

$$\vec{\delta}_1 = \frac{a}{2}\left(1, \sqrt{3}\right), \qquad \vec{\delta}_2 = \frac{a}{2}\left(1, -\sqrt{3}\right), \qquad \vec{\delta}_3 = a\left(-1, 0\right), \qquad (1.3)$$

while the six second-nearest neighbors are located at

$$\vec{\delta}_1 = \pm\vec{a}_1, \qquad \vec{\delta}_2 = \pm\vec{a}_2, \qquad \vec{\delta}_3 = \pm\left(\vec{a}_2 - \vec{a}_1\right). \qquad (1.4)$$

The two points K and K' hold particular importance for the physics of graphene at the corners of the graphene Brillouin Zone (BZ). The positions of these Dirac points

in momentum space are given by:

$$\text{K} = \left(\frac{2\pi}{3a}, \frac{2\pi}{3\sqrt{3}a} \right), \qquad \text{K'} = \left(\frac{2\pi}{3a}, -\frac{2\pi}{3\sqrt{3}a} \right). \qquad (1.5)$$

1.1.3 Electric properties of graphene

For calculations regarding the energy bands, the tight-binding approximation is used. This ensures that only the nearest and second-nearest neighbor atom interactions are considered in the calculations.

The energy bands have the form:

$$E_\pm (k) = \pm t\sqrt{3 + f(k)} - t'f(k), \qquad (1.6)$$

where $t(\approx 2.8\,\text{eV})$ is the nearest-neighbor hopping energy (energy required to hop between different lattices) and t' the second-nearest neighbor hopping energy (hopping in the same sublattice). The value of t' depends on the circumstances and accuracy of the calculations, but the value according to cyclotron resonance experiments is $t' \approx 0.1\,\text{eV}$.
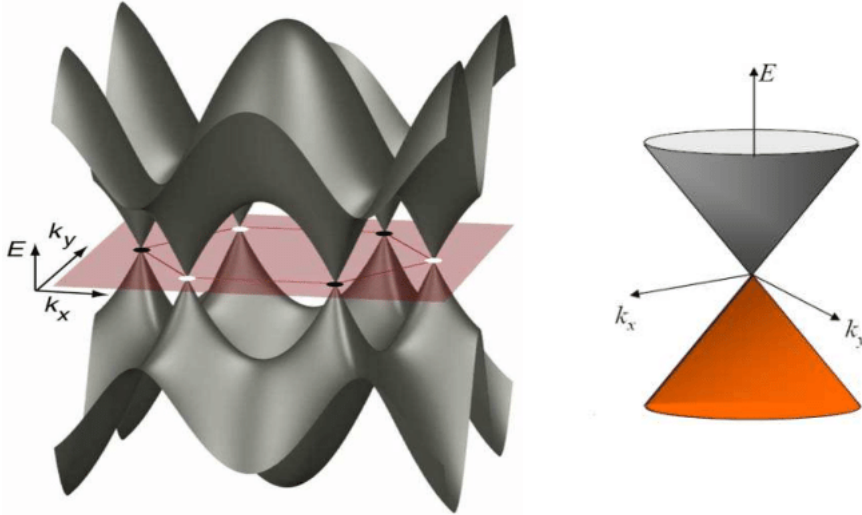

Fig. 1.2: Electronic dispersion of graphene throughout the Brillouin zone, the zoom depicts the structure on the Dirac cone near the Fermi level, adapted from [4].

For the dispersion relation around the Dirac point K, the following approximation can be used

$$E_\pm (\vec{q}) \approx v_F |\vec{q}|, \qquad (1.7)$$

where q is the momentum measured relatively to the Dirac points and v_F is the Fermi velocity, with a value of $v_F \simeq 1 \times 10^6\,\text{m/s}$. Here the wave vector $\vec{k}$ takes the form of $\vec{k} = \text{K} + \vec{q}$, where $q \ll \text{K}$.

1.1.4 Chemical vapor deposition

One of many problems in physical experiments with graphene, is its preparation. There is a variety of methods of graphene preparation, all with their respective benefits and drawbacks. The two main categories of graphene preparation methods are the top-down and bottom-up methods.

One of the most important bottom-up methods of graphene preparation is chemical vapor deposition (CVD). Using high temperatures to decompose various hydrocarbons, namely methane, we can grow graphitic layers on heated substrates. These substrates are usually transitional metals, which act as a catalyst in lowering the energy barrier of the reaction and they also determine the graphene deposition mechanism.

Metals with high carbon solubility (such as Ni and Fe) dissolve the carbon into themselves at high temperatures. As the substrate is cooled down, the carbon segregates to the surface to form graphene sheets [5].

However, when it comes to metals with low carbon solubility (such as Cu) [6], carbon atoms nucleate and expand around to form graphene domains. The growth process ends when the substrate is fully covered by the graphene layer. This is called a "self-limited surface deposition" growth mechanism.

The difference in the process behaviour, depending on the choice of the substrate, can be observed in the figure 1.3.
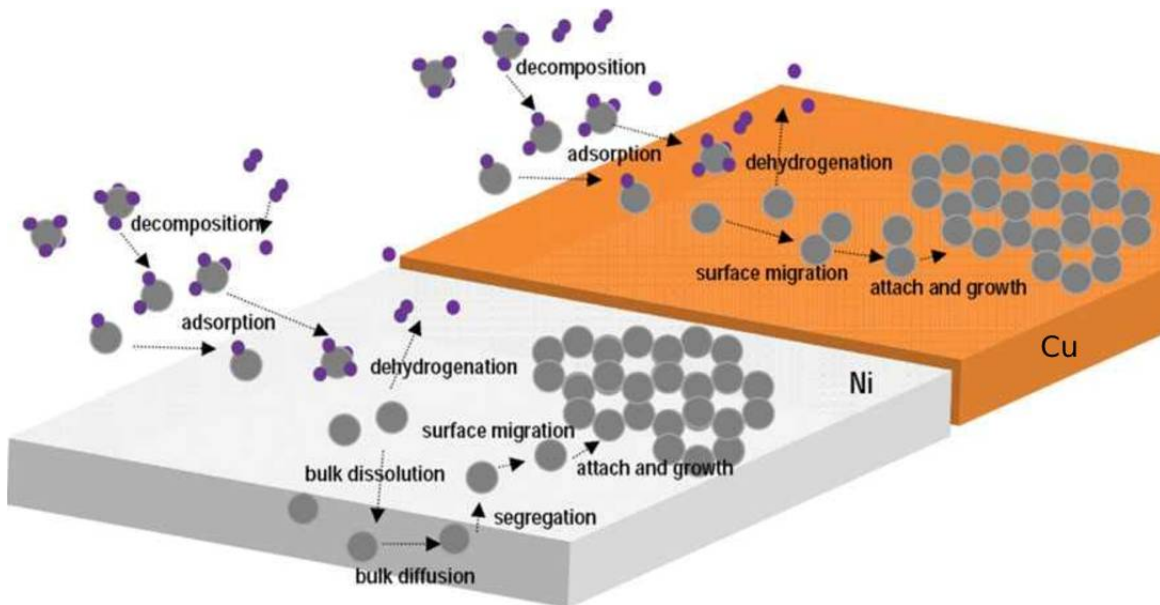

Fig. 1.3: Chemical vapour deposition of graphene on Ni and Cu substrates, adapted from [5].

The growth of graphene using copper as the catalyst substrate proves to be the most popular method for preparing large-area, high quality monolayer graphene. This is due to its low carbon solubility in copper, which offers a path for growth.

1.1.5 Mechanical exfoliation

This method of graphene preparation belongs into the top-down category. The resulting graphene samples are sub-ideal for covering larger surfaces, because the yield is far lower than in other methods. The added drawback is that it is also a slower and more work demanding method. On the other hand, the benefit of this method is the acquisition of samples of high grade purity, ideal for laboratory experiments and prototype technologies [7].

The method involves using a scotch tape on Highly Orientated Pyrolytic Graphite (HOPG) to remove several layers of graphene. The tape assists in breaking the van der Waals bonds to remove the layers of carbon. For every mono-layer of graphene, one needs to exert $3 \cdot 10^{-4}$ nN worth of force for every mm^2 of area [8].

After the initial exfoliation, the process is repeated, but this time on the layers of graphene on the initial scotch tape (fig. 1.4a). This process is continued (fig. 1.4b), until mono-layers of graphene are observed on the tape in the form of islands of carbon with micrometer dimensions. When this stage is achieved, the tape is placed on the target surface (typically Si or SiO$_2$ substrate) (fig. 1.4c). The graphene samples then stick to the target surface at random positions (fig. 1.4d).

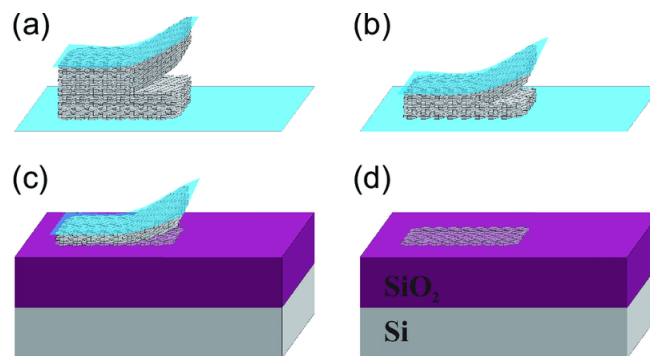The process is depicted in the figure 1.4:

Fig. 1.4: Mechanical exfoliation of graphene on a SiO$_2$ substrate, adapted from [9].

It is important to stress the fact that the samples are often too small to cover all targets (such as the electrodes on a Hall bar). In instances, where it is a must to cover larger areas, it may be necessary to look into other methods of graphene preparation (such as CVD).

1.2 Atomic force microscopy

1.2.1 General overview

Atomic Force Microscopy (AFM) is a type of scanning probe microscopy, which has a nanometer scale resolution. This is possible due to the fact that it uses various piezoelectric elements, which are capable of making accurate movements during the scanning process. Some microscopes are capable of imaging the precise topography of a sample on the scale of individual atoms [10].
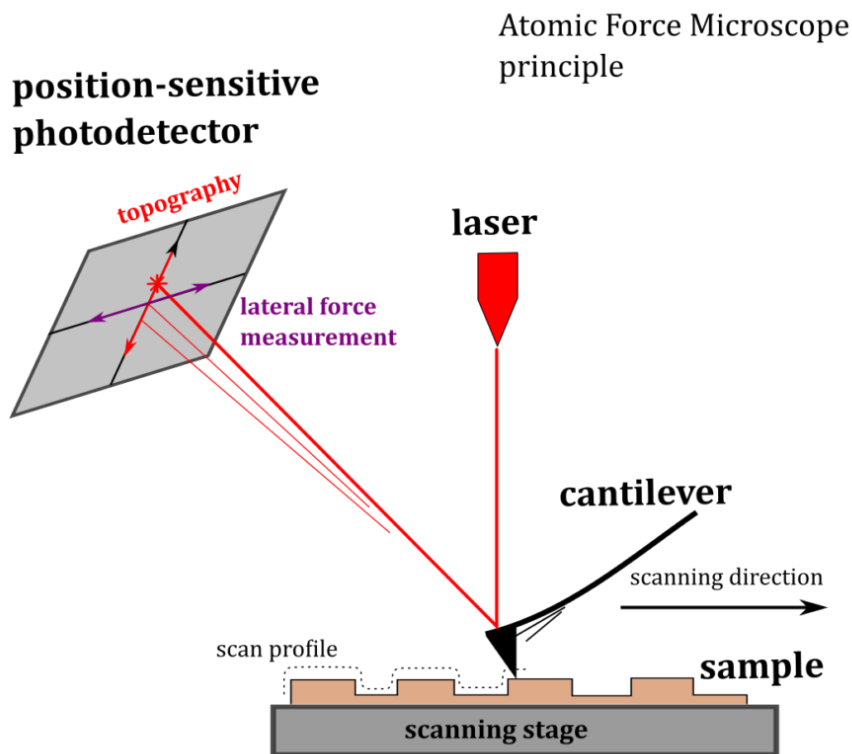
Fig. 1.5: The principle of AFM, adapted from [11].

The cantilever with the tip is connected to the rest of the probe chip, which has a laser beam pointed at its end. As the laser is reflected into the photodetector, the input is converted into an electric signal, which the computer processes. The cantilever moves in an up and down motion, while being able to twist. The result is an image of the profile, which depicts the surface's topography [11].

1.2.2 Probes

The accuracy of AFM technologies is largely owed to the design of the probes. At the end of the cantilever is the tip, which is, at its smallest dimension, only several to tens of nanometers in diameter. The cantilever itself is also much too small for practical manipluation (in the tens of micrometers). That is why it is connected to the cantilever holder [12]. These chips hold the cantilever in place and allow laboratory personnel to move and replace probes in the scanning head of the AFM with the use of tweezers.

The cantilevers and tips themselves can have different shapes and sizes, specialized for different purposes. Most cantilevers are rectangular in shape, but other types exist. For example, most diamond coated probes are designed to withstand lithography by plowing (dynamic plowing) and therefore they can employ the use of a triangular cantilever with a thicker tip.

Most AFM probes are made of silicon (Si). To increase detection capabilities or other properties of the probes, some make use of coatings. For higher precision in the measurement of electric properties of samples, golden (Au) coatings are used. For higher stiffness, titanium nitride (TiN) is recommended and for higher resistance, diamond coated probes [13]. Although most of these coats are applied to the tip only, some coats are added to the cantilever as well, to increase the reflectivity for the laser.

For one to get the highest quality images from the AFM device, the probes need to be taken extraordinary care of during the insertion process.
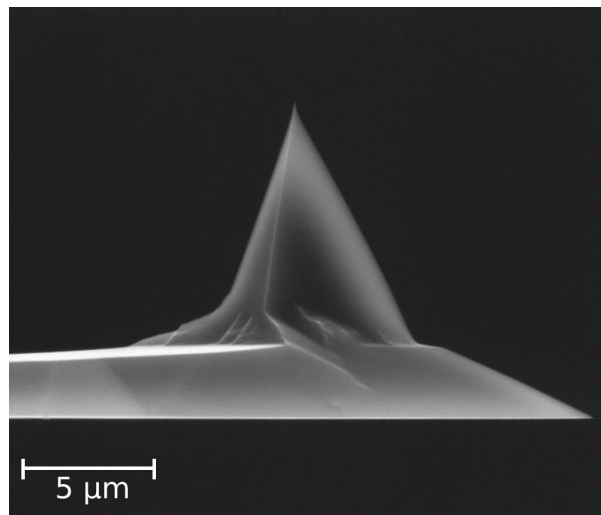

Fig. 1.6: Tip of a non-contact gold coated probe (NSG10/Au), adapted from [14].

1.2.3 Imaging modes

Contact mode

The contact mode of an AFM drags the cantilever across the sample surface. Using the feedback signal to keep the tip at a constant position, the images can be processed. The other method is to observe the deflections of the cantilever itself [15].

In this mode, stiffer cantilevers are prone to breakage. Therefore, softer probes with a lower spring constant k are used. The relationship between displacement z and the resulting force F follows Hooke's law [16]:

$$F = -kz. \tag{1.8}$$

Non-contact mode

The non-contact mode, as the name suggests, works without contacting the surface of the sample. Instead, the cantilever is oscillated at its resonant frequency (where the amplitude is a couple nanometers). When the tip of the cantilever interacts with long range forces coming from the sample (such as the van der Waals interaction), the resonant frequency decreases. The feedback loop system maintains a constant amplitude or frequency, by adjusting the distance between the tip and the sample. The distance is recorded for every point on the targeted scan area, thus creating the topographic image [17].

The benefits of non-contact measurement include the fact that the tips of the cantilevers do not get contaminated or dull as often. After several scans in contact mode, the images worsen significantly in terms of resolution [18]. This scenario is less frequent in non-contact mode. However, the cantilevers can still be broken when subjected to high amplitude oscillations. The cantilevers can also be coated with stiffer materials, since they are not required to copy the surface profile of the sample directly.

Tapping mode

In tapping mode, the cantilever does come into contact with the surface, but it is not dragged alongside it either. The cantilever is oscillated at its resonant frequency and the amplitude and frequency are maintained, using the feedback loop. The minor changes in altitude are recorded as a signal at each point and processed into an image [19].

Although, the probe contacts the surface, the damage done to the tip and sample is to a degree mitigated. This is due to the fact that the duration of time, when the force is applied, is short.

1.3 Kelvin probe force microscopy

1.3.1 General overview

Mapping the surface potential of a sample proves to be a critical endeavor in the description of electrical capabilities of nano-materials. Kelvin Probe Force Microscopy (KPFM) is one member of available methods of doing just that.

KPFM gives information about the surface potential of a sample surface, thus providing us with information about the electrical properties of the target sample. KPFM can also be used to measure the work function of the given material [20]. The work function, in solid state physics, is defined as the energy needed to free an electron from the Fermi level in a solid to vacuum, which means that the work function is a characterization of the surface, not the whole solid. This means, KPFM can only be used to describe the surface and near-surface only.

To operate, KPFM needs a thin electrically conductive material coating on the cantilever of the probe. KPFM operates in amplitude modulation mode, which is a type of dynamic force mode (tapping mode), where the cantilever is oscillated at its resonant frequency.

There are two essential setups for KPFM to operate in: single and dual pass. In the single pass setup, the tip passes the over the sample surface only once at a constant height. During which an AC voltage is applied to the cantilever (with a frequency other than resonant). This creates an oscillating electrostatic force between the tip of the cantilever and the sample, which is measured by a lock-in amplifier. Then a DC voltage is applied to counteract the potential and prevent the cantilever from oscillations. This DC voltage is the recorded and mapped as a measure of the contact potential difference between the tip and the sample surface.

The benefit of the single pass mode is that the tip is closer to the sample, increasing the sensitivity and resolution of the Kelvin force measurement. But as a trade off, the spatial resolution is downgraded. Since the probe only passes the sample surface only once, this setup is ideal in time sensitive measurements, since it is the fastest.

In the dual pass setup, the probe passes over the sample twice over every line. During the first pass, the height of the sample is measured, thus getting a topographic image of the sample. In the second pass, the tip is lifted by a set amount by the user (as to not crash into the sample, but, also close enough that stray capacitance from the lever does not interfere with the measurement). The process of the second pass is analogous to the single pass setup described above.

The slower scan rate and double passing can complicate the measurement of time sensitive tasks. On the other hand, this setup provides the best spatial resolution

and thus can offer an immediate comparison between the KPFM image and the topography.

1.3.2 Applications and examples of KPFM

In the figure below, we can see a single pass KPFM measurement of a multi-layer graphene flake on top of a silicon (Si)- silicon dioxide (SiO_2) substrate. The contrast in the image shows the surface voltage of the various layers and hotspots on the sample. The thin flakes on top (blue) have a higher contact potential, than the lower (green) layers.
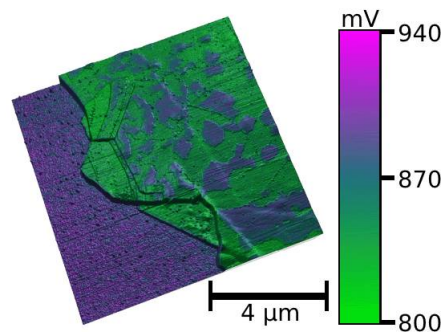

Fig. 1.7: Single pass setup of KPFM measurement of a graphene flake, adapted from [20].

In the next figure, we have an example of a dual pass KPFM setup scan on an insulating oxide. In this sample, local charges were placed in the shape of the Swiss cross. In the topography image on the left, there is no sign of such a pattern. However, the KPFM image on the right reveals placed local charges, by measuring the surface potential.
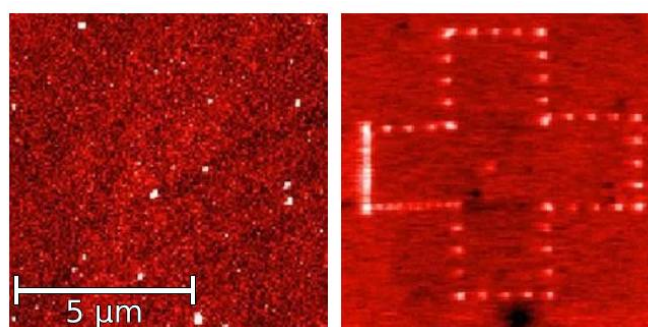

Fig. 1.8: Dual pass setup of KPFM measurement of an insulating oxide with placed local charges in the pattern of the Swiss cross, adapted from [20].

2 Research

The goal of this literature research is to find different ways of graphene interruption and quantum point narrowing. While also tackling the observation of charge diffusion, using KPFM.

2.1 Graphene interruption

Kun et al. [21] used the method of cleavage lithography to interrupt the graphene lattice. By exploiting the AFM's capability to determine the crystallographic orientation of the lattice, they were able to interrupt the graphene by pressing down onto the sample and dragging the AFM tip into the sample surface to a predetermined deflection. Their samples consisted of graphene prepared by micromechanical exfoliation on a silicon substrate with 285 nm SiO_2 capping layer. By revealing the high symmetry lattice directions of the graphene sheet, they were able to identify the most ideal path for the lithography. By picking the direction, where the carbon atoms are alternating (in a armchair/zigzag manner), graphene can be cut (cleaved) more easily. This also includes the fact that the nature of the cuts is more precise, with less tearing occurring around the lithography impacted area.

The graphene cleavage lithography itself is a technique, where the cantilever tip presses into the sample and ruptures the graphene by indentation. Due to graphene's outstanding tensile strength, up until a depth of approximately 1.5 nm, the material is only stretched. After the limit depth, the chances of graphene rupture increase dramatically.
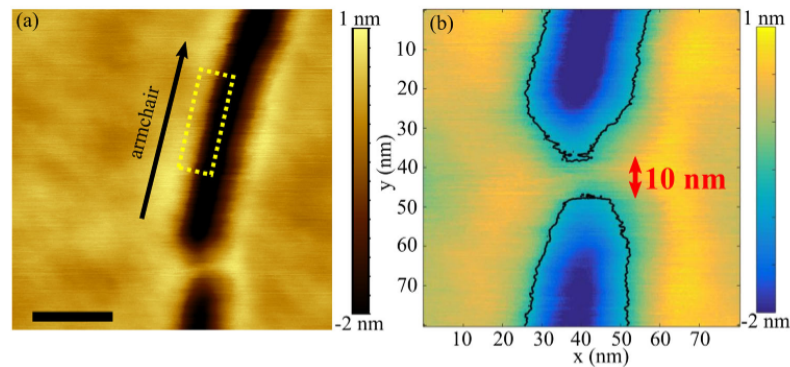

Fig. 2.1: High resolution AFM cleavage lithography of graphene quantum point contacts. a) Topographic tapping-mode AFM image of a 10 nm wide graphene constriction. Scale bar: 500 nm. b) Locating the graphene edges (marked by the black line). Adapted from [21].

Lu et al. [22] used their AFM in contact mode, to scratch their graphene oxide samples. The samples were prepared using the modified Hummers method from graphite powder, which were assembled on a Si/SiO_2 substrate. The Si AFM tip they used to interrupt the graphene oxide layer had a set point of $3\,V$, which they used to create graphene oxide-free gaps. If a smaller force (such as set point $= 1\,V$) was used, the graphene oxide could not be completely scratched. However, when they used a greater force (such as set point $= 5\,V$), the force destroyed the Si/SiO_2 substrate.

This method was described by them as very flexible and convenient for the fabrication of different patterns of graphene oxide. They managed to scratch away gaps as thin as $56\,nm$.

Another method of gap creation was also described in the article: local anodic oxidation (LAO) lithography. For LAO lithography to be used, it is necessary for the substrate to be conductive, in order to generate the needed current between the AFM tip and the substrate when a bias is applied. The area around the graphene sheets in contact with the AFM tip was oxidized and a new bumpy structure was formed on both sides of the trench generated by the AFM. One of the advantages of their method, was that their choice of substrates was more flexible. For them, it is not necessary for the used substrate to be conductive.

2.2   Graphene charging

Konečný et al. [23] observed the effect of relative humidity (RH) on electron hopping by isolating graphene samples, charging them and mapping the surface voltage using KPFM (using NSG10/Au probes) at different time frames. They used conventionally CVD grown graphene on a Si/SiO_2 substrate and used a diamond coated probe to separate their graphene islands from the grounded graphene around. Using the gold coated probe, they charged the graphene sheet with a bias voltage of $\pm 1.5\,V$ for $2\,minutes$. Finally, they measured the surface potential using KPFM.

In the other part of their experiment, on one of the sides of the graphene island, they separated the graphene from the grounded one by a gap and repeated the charging and surface voltage mapping. The mapping was repeated several times after the initial charge at a constant RH. After each experiment, they let the sample discharge overnight or after several hours at high ($>70\,\%$) RH. Then they set a new RH and repeated the process. The aforementioned gap width was increased, after each completed experiment, in the following sequence: $(40, 300, 1000, 2000)\,nm$.

By the end of their experiments, they found that the diffusion of charge from the charged sheet to the surrounding SiO_2 substrate and the nearby sheet grows exponentially with the increase of RH. The resistivity of silicon however, came out

to be lower than the values listed in their used literature. Their theory for this phenomenon is that there may have been some carbon contaminants, which aided the diffusion, inviting further research into different methods of lithography (such as optical or electron beam lithography) than just mechanical.

For a better understanding, we can see the schematic of their experimental setup in the following figure 2.2:
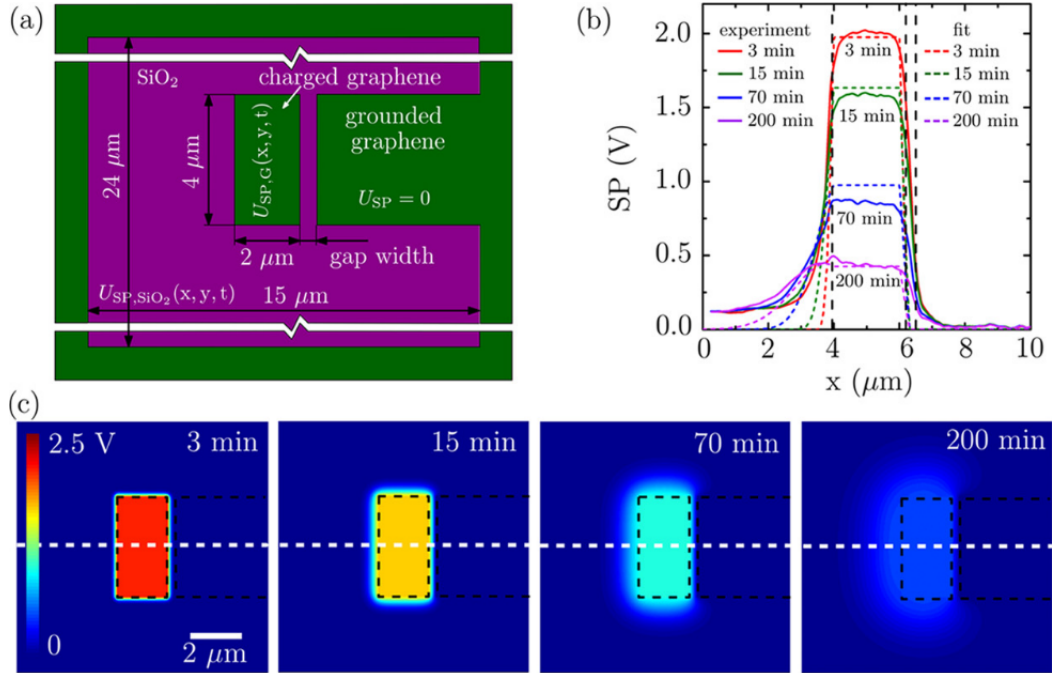

Fig. 2.2: a) The schematic illustration of simulated sample geometry. b) The measured surface potential (solid line) at 25 % RH and the corresponding fits taken at: 3 minutes, 15 minutes, 70 minutes and 200 minutes, where the gap width between the graphene sheet and the graphene island is 300 nm. c) The corresponding simulated surface potential time evolution. Adapted from [23].

3 Thesis results and experimental setup

Firstly, we needed to prepare samples, on which we could start forming our nano-structures. Then, we set up the AFM for the mechanical lithography, which we used for the mechanical lithography of our samples. Finally, we charged the graphene with a bias voltage from the AFM cantilever tip and measured the surface potential, using KPFM.

3.1 Chip preparation

The graphene we used during our experiments was prepared by a standard CVD method on copper sheets. The procedures described below concern only the repositioning of graphene and the preparation of the target surfaces.

We were using a silicon (Si) wafer with a $285\,\text{nm}$ layer of silicon dioxide (SiO_2). After a close inspection for artifacts and other damages, we chose an ideal wafer from the available selection.

To procede, we needed to spincoat the wafer (to prevent contamination during the wafer cutting process). This included annealing the wafer at $100\,°\text{C}$ for $15\,\text{minutes}$ to remove any water droplets and particles. Then, we manually added poly(methyl methacrylate) (PMMA), specifically PMMA $50\,\text{K}$ (AR-P 639.04, by the company Allresist) using a pipette on the top layer. After that, we set the spincoater for 2200 rotations per minute for one minute. Hardening the evenly distributed PMMA at $150\,°\text{C}$ for $5\,\text{minutes}$ was necessary, to be able to add a second layer of PMMA, this time: PMMA 950 (AR-P 679.04, by the company Allresist). The spincoating was analogous to the previoes procedure. For the removal of any PMMA droplets on the bottom half of the silicon wafer, we used laboratory tissues and acetone.

For the graphene to be placed on top of the Si wafer, first, the wafers need to be cut into appropriately sized squares. A diamond tipped scribe is used to scratch the bottom half (Si side) of the wafer, following the lattice of the silicon atoms, to create lower resistance. Then a moderate amount of hand pressure is used on plastic clamps to break the wafer down. Repeating the process until we have our desired samples. The products are then washed off in acetone and isopropyl alcohol (IPA), to remove any remaining silicon dust from the breakage.

Using reactive-ion etching (RIE), we were given plasma-etched samples, which uses oxygen plasma to remove organic contamination deposited on wafers. Before and after each use of the RIE machine, it needs to be thoroughly cleaned.

The pocedure for removing the copper below the graphene and PMMA, is etching. First, the copper is cut up into suitable sizes (usually squares of $5\,\text{mm}$ by $5\,\text{mm}$)

using laboratory scissors. For straightening the copper squares, two tweezers are advised. For the etching, we used $1\,M$ solution of $Fe(NO_3) \times 9\,H_2O$. Putting the flakes of copper into the solution, so that the graphene is on the top, without touching the solution for a maximum of $2\,$hours. After the dissolution of the copper, the graphene and PMMA flakes are transferred into deionized water four times, in different containers. Then the flakes are placed into hydrochloric acid (HCl) of $5\,\%$ concentration for $5\,$minutes to remove any remaining metallic contaminants. The process with the deionized water is again repeated. Finally, the graphene and PMMA is submerged into ethanol (without letting it float to the bottom of the container), to remove the contaminated water.

The silicon substrates are annealed at $180\,°C$ for $45\,$minutes. To remove any organic contaminants, the RIE machine is used once more. Then, the graphene is removed from the ethanol and placed on the prepared Si wafer. To remove any remaining liquid, we used pressurized nitrogen to dry and blow it off. We then let it dry further overnight.

The next logical step was to remove the PMMA layer from the graphene. In $5\,$minute intervals, we increased the annealing temperature in the following sequence: $40\,°C$, $60\,°C$, $80\,°C$ and $105\,°C$. Then, we placed the samples in acetone for $1.5\,$hours, successively into acetone at $52\,°C$ for $60\,$minutes. Upon taking the samples out, we cleaned off any remaining acetone with the use of IPA. As a last step, we washed them off in ethanol one final time and let the samples dry.

In order to skip the gold (Au) wire bonding process, we were given an earlier batch of samples, prepared in an analogous fashion as ours.

In the following figure 3.1, we can observe our prepared samples (left) with the PMMA still intact, for better visibility. The two-contact chips (right) are the ones given to us and the ones we conducted our research on.
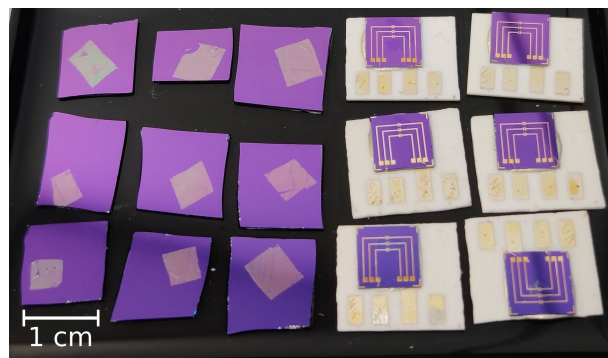

Fig. 3.1: Our prepared graphene samples on Si/SiO_2 wafers (left) and the two-contact chips (right).

Although, we used $Fe(NO_3)$ for the dissolution of copper, other alternatives exist as well, such as: $0.1\,M$ solution of $(NH_4)\,S_2O_8$. However, that would have taken around $2\,$days to remove the copper completely, due to the low concentration.

3.2 AFM setup

For all measurements, the calibration of the AFM is crucial in obtaining quality images, protecting probes from breakage and preventing unnecessary damage of the samples.

After turning on the AFM and preparing the vibration compensator of the table, we can begin the insertion of the chosen probe. For our measurements, we first inserted the diamond coated probe (DCP 20). The laser is turned on automatically upon opening the control software on the connected computer. Using the contraptions on the head, we roughly aim the laser at the cantilever of the probe, until we see interference images, resulting from the obstructed laser. The samples are then placed on the magnetic holder. For safety reasons, the holder is lowered, to protect the sample from being scratched. The head is then placed into its designated place.

Using the camera, we can adjust the laser more carefully, so that it is aimed just below the end of the cantilever (this area provides high reliability for reflectivity and accuracy). Using the software, we aimed the laser beam reflecting from the cantilever of the probe into the middle of the photo-diode.

As our laser preparation has concluded, we can turn on the vibration compensator of the table. The next part of the calibration depends on what scan mode we want to be using.

To set up the non-contact mode, we need to find the resonant frequency of the given probe. This can be done using the software, by selecting the resonance test interval from $50\,$kHz to $500\,$kHz. This provides us with a bell curve, where the apex of the curve is the resonant frequency, which we are going to be offsetting to an appropriate amount. To prevent the probe from being damaged, the amplitude of the oscillations is adjusted by setting the feedback gain to 0.2.

In case we wish to scan in contact mode, we lower the set point to 2 and increase the feedback gain to 0.5 (in case of high oscillations, the value can be less, however, not < 0.1). For contact mode measurements, contact mode probes are necessary.

Now that we have our settings in order, we can approach the sample using the software. The magnetic holder with the sample begins to get closer to the probe and slows down its movement rate as it approaches. If the oscillations are excessive, the feedback gain needs to be adjusted to prevent to probe from being damaged any further.

To adjust the position of the cantilever on the sample, we simply back away and adjust the sample position with the fiddles on the AFM, while observing the movement on the camera feed.

3.3 Nano-structures

After the calibration is complete, we can begin scanning the surface of the sample. As mentioned above, the probe we are using is a DCP 20, which is a non-contact probe.

Using the scanning capabilities of the AFM software, we can begin to scout out a suitable area for our structure preparation. To do this, we are setting the scan for an area of $(70 \times 70)\,\mu m^2$ at point number of (256×256) at a frequency of $0.5\,Hz$, so that the cantilever does not oscillate side-to-side too much. Upon finding an area of $(5 \times 5)\,\mu m$ with the least amount of artifacts and an even distribution of graphene, while still staying close to one of the electrodes of the sample chip, we can begin a detailed scan.

Our goal is to create a separate graphene sheet from the grounded graphene around it, by making a $(3 \times 3)\,\mu m^2$ square are desolate of graphene (a graphene channel), except for the middle $(1 \times 1)\,\mu m^2$ graphene island in the middle. But first, we need to set the bounds of the channel and of the island. To achieve this, we select the "litho" tab of the software and using the vector option, we can draw the square channel. After several iterations of the same experiment, it is recommended that the user draws another (neighbor) parameter around the graphene island. The reason for this, is that in the next steps, there is a likely-hood, that the graphene island might get dragged away, which is not our intention. To actually cut into the graphene sample, contact mode is selected and the set point value is increased to 10 (which is roughly equal to $1000\,nN$ of force). The reason we are allowed to use a non-contact probe in the contact configuration, is that we are using a DCP 20 probe, which is more than capable of withstanding mechanical lithography of graphene. The reason behind this, is the geometry of the cantilever, which is triangular in shape, which makes it more resilient. Added to that is the fact that the tip is diamond coated, which makes it possible to break the covalent bonds of the graphene, without excessive dulling of the tip. To increase the efficiency of the lithography, we are setting the velocity of the scan to $0.3\,\mu m/s$.

After the borders are drawn, a scan is required to inspect the image (the scan is conducted in semi-contact mode). To form the channel, we simply select an arbitrary (non-square shaped) scan and position the scan area at the sides of the channel, where the graphene needs to be removed. In our case, for every μm^2, we used a resolution of (64×64) and a speed of $1\,\mu m/s$. To plow the graphene away

from the channel, we switched back to contact mode and used the appropriate scan direction, to remove the debris from the channel (removing the remaining debris properly is crucial for the experiment).

This process was repeated until the channel and graphene island were formed. In our case, we managed to make two such structures, where the next part of the experiment was conducted.

The end result of our endeavors can be observed in the following height scan image (figure 3.2)
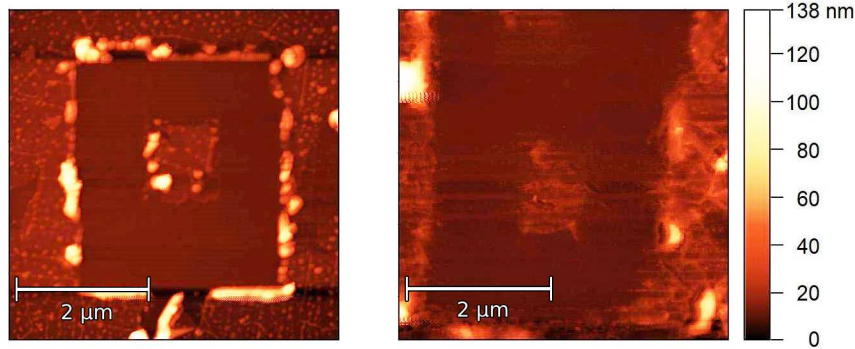

Fig. 3.2: Height scan of two graphene channels with graphene islands at their centers (scans made with NSG10/Au).

The lower image quality of the second image (fig. 3.2, right) can be attributed to the fact, that the point number was set at a lower resolution of (256×256), whereas the first one boasts a resolution of (512×512).

3.4   Final results

For the measurement the surface voltage we swapped the probe. This time, a gold coated, non-contact probe (NSG10/Au) was inserted into the head of the AFM. After the calibration process and finding the graphene channels, we started our final stage of measurement.

The probe tip was aimed above the graphene island in the middle of the structure and we set the bias voltage of the tip to 8 V. To actually charge the graphene, we had to switch to contact mode. Since we are not moving the cantilever, only simply touching the surface, there is no danger of damaging the equipment. After contact, we waited a total of 60 seconds to allow proper charging. Then, we retracted the tip from the surface and quickly switched back to semi-contact mode, while also selecting the "Kelvin probe force microscopy" option. Finally, we scanned the area in question multiple times for both structures.

In our first structure, we did not influence the surrounding relative humidity (RH), which was measured at 36 %. The surface voltage measurements were conducted in the following intervals from the point of charging: 10 minutes, 25 minutes and 40 minutes. In the following figures 3.3, we can observe the results:
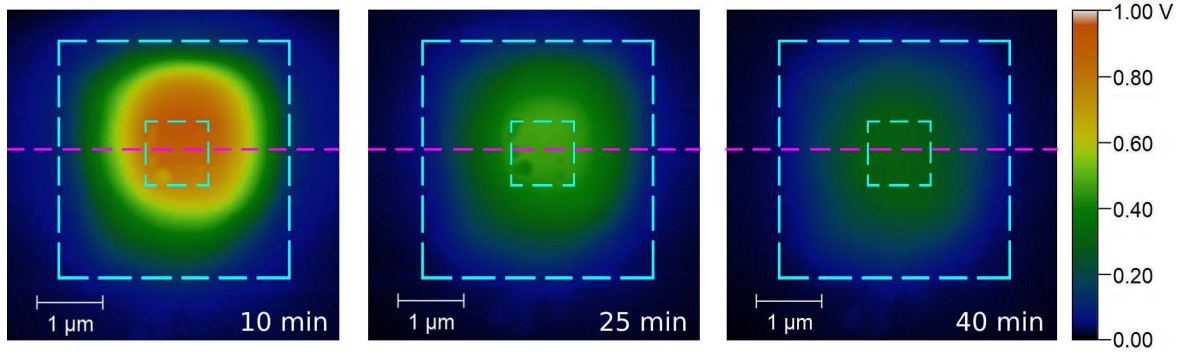

Fig. 3.3: Heat map of surface voltage on the first nano-structure in different time intervals (RH ≈ 36 %).

The borders of the graphene layer are marked with a cyan segmented line, where the space between the borders contains no graphene. We can see that the maximum surface potential is concentrated in the area of the graphene island with minor disruptions. The disruptions are presumably caused by accumulated carbon debris from the mechanical lithography, which we can clearly observe in figure (3.2, left). As the charge dissipates into the environment, it encounters the SiO_2 channel, where the resistance is much higher [23]. The channel acts as an insulating barrier, despite its $1 \, \mu m$ width. The charge carriers (electrons and holes) that manage to overcome the barrier are absorbed by the surrounding graphene sheet, which is electrically grounded.

The charge dissipation can also be observed on a graph (figure 3.4), where we took the profile of a straight line. In our case, we chose the line segment roughly in the middle, marked with the magenta colored segmented line. The irregularities in the maximal surface potential can clearly be seen, due to the above mentioned debris. As we move to the graphene channel, the profiles start to resemble a bell-curve like shape, where the surface potential drastically decreases. As the surface potential measurement approaches the electrically grounded graphene, the voltage further decreases and approaches the zero value. We can also notice, that the potential differences between the measurements themselves decrease over time. We can assume that the charge dissipation speed exhibits an exponential trend, which is supported by previous experiments [23].
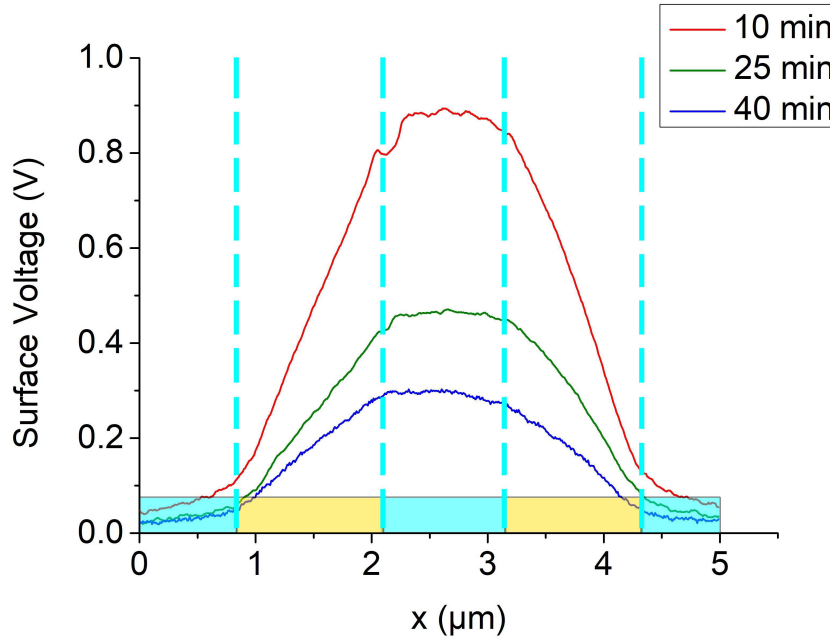
Fig. 3.4: Surface voltage dissipation of the first nano-structure in different time frames (RH $\approx 36\,\%$). The cyan rectangles represent the presence of graphene and the yellow rectangles represent the channel (SiO_2).

In the second structure, we used a humidity chamber to create a nitrogen rich environment, where we managed to get the RH down to $1\,\%$. The same bias voltage was used, however, we scanned the sample in different time intervals: $5\,minutes$, $15\,minutes$ and $30\,minutes$. The resulting measurements can be observed below (figure 3.5):
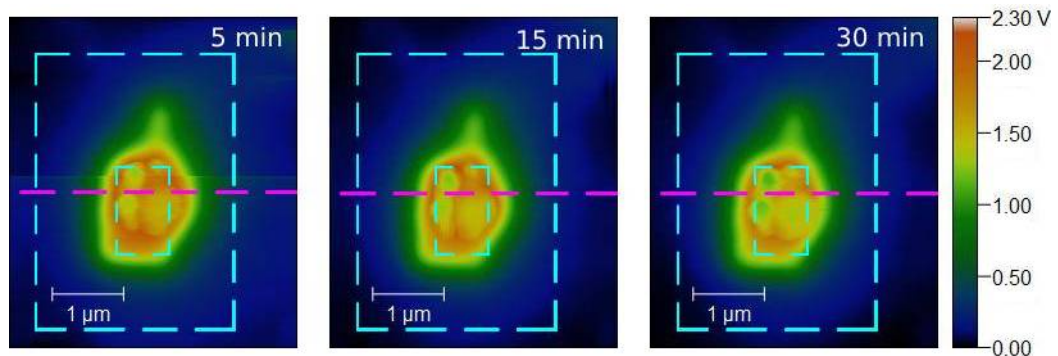

Fig. 3.5: Heat map of surface voltage on the second nano-structure in different time intervals (RH $\approx 1\,\%$).

This time, the graphene borders, again marked by cyan colored segmented lines,

are unfortunately not convenient square shaped, but rather rectangular. In contrast with the measurements at 36 % RH, we can clearly observe that the charge remained highly concentrated in the vicinity of the graphene island even after 30 minutes. This is due to the fact that a lower amount of water molecules were present in the environment and as a result, the resistivity of the SiO_2 channel increased [24]. The irregularities observed in the surface potential of the graphene island are not necessarily caused by an accumulation of debris (as evident from the height scan in figure 3.2, right), but rather by unintentional damage, which exposes the SiO_2 layer. This causes spikes in resistivity, resulting in localized lower surface potential levels.

The respective graph (figure 3.6) was sourced from the line segment marked with a magenta colored segmented line in figure 3.5.
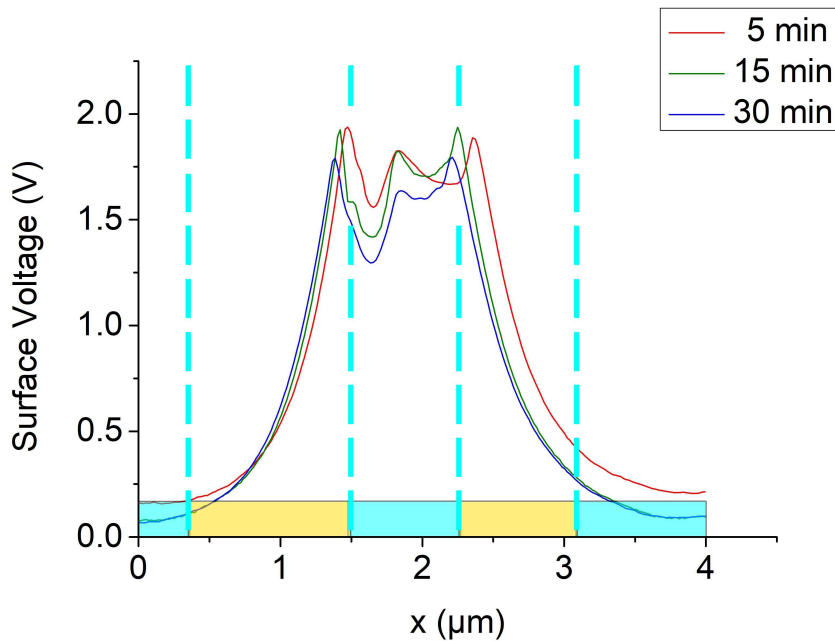

Fig. 3.6: Surface voltage dissipation of the second nano-structure in different time frames (RH ≈ 1 %). The cyan rectangles represent the presence of graphene and the yellow rectangles represent the channel (SiO_2).

We can observe that the surface potential around the graphene island is less even, than in figure 3.4. We can presume that the occasional damage causes a considerably bigger disruption in charge distribution than excess carbon debris. As we approach the SiO_2 channel, at a much lower RH of 1 %, the surface potential drop is even more prominent than in figure 3.4. However, the behaviour of the surface potential around the edges of the grounded graphene is analogous to the aforementioned figure.

Conclusion

In this bachelor's thesis, we focused on the preparation of nano-structures on graphene, namely using mechanical lithography as our chosen method of graphene interruption.

At the beginning of the thesis, we discussed the basic characteristics of graphene and their preparation process, we described AFM and KPFM and their essential functions for our experiments.

In the research part of our thesis we looked into previously conducted experiments that were most relevant to our topic and we briefly described their final accomplishments during their work.

In the experimental part of the project, we roughly described the preparation process of the Si/SiO_2 substrate samples and the graphene (made with a standard CVD method) repositioning procedure from the copper foils. Then we described the AFM setup process and its various intricacies. We, then moved onto the nano-structure fabrication, using the AFM. Here, we managed to form two working structures, which were each meant to be a $(3 \times 3)\,\mu m^2$ area without graphene, while leaving the middle $(1 \times 1)\,\mu m^2$ area intact. This effectively created a SiO_2 isolating barrier (channel) between the graphene island and the surrounding grounded graphene. Then we charged the graphene island with a bias voltage at the cantilever tip at $8\,V$ for $1\,minute$. Subsequently, we measured the surface voltage of the graphene island and the general area surrounding it in different time frames using KPFM. The produced images depict the slow dilution of the uneven charge across the structures in time. To observe the charge dissipation even better, we took the profiles from the middle of the structures and put them in a combined graph to emphasize the difference relative humidity makes.

The first nano-structure exhibited an uneven surface potential around the area of the graphene island, which were presumably caused by accumulated carbon debris. However, these disruptions were surpassed by the surface potential drops on the second nano-structure's graphene island, where the damage on the graphene caused the SiO_2 substrate to be exposed. Paired with the low RH values $(1\,\%)$, the sharp decreases in surface potential were amplified.

Bibliography

[1] CASTRO NETO, A., GUINEA, F., PERES, N., et al. The electronic properties of graphene. *Reviews Of Modern Physics.* AMER PHYSICAL SOC, **2009**, vol. 81(1), p. 109 – 162, [cit. 2021-5-17]. ISSN 0034-6861. Available from: doi:10.1103/RevModPhys.81.109.

[2] LEE, C., WEI, X., KYSAR, J. W., et al. Measurement of the elastic properties and intrinsic strength of monolayer graphene. *Science (New York, N.Y.).* **2008**, vol. 321(5887), p. 385 – 388 [cit. 2021-5-18]. ISSN 00368075. Available from: doi:10.1126/science.1157996.

[3] METTEN, D. *Probing the opto-electronic and mechanical properties of suspended graphene membranes by Raman spectroscopy.* University of Strasbourg. Institut de Physique et Chimie des Matériaux de Strasbourg, **2016**.

[4] KIMOUCHE, Amina. *Toward novel hybrid materials based on epitaxial graphene: Controlling the formation of defects and using them for intercalation.* Département Nanosciences de l'Institut Néel. Université de Grenoble, **2013**.

[5] CHEN, X., ZHANG L. and CHEN, S. Large area CVD growth of graphene. *Synthetic metals.* Elsevier B.V, **2015**, vol. 210(PA), p. 95 – 108 [cit. 2021-5-17]. ISSN 0379-6779. Available from: doi:10.1016/j.synthmet.2015.07.005.

[6] REINA, A., JIA X., HO, J., et al. Large area, few-layer graphene films on arbitrary substrates by chemical vapor deposition. *Nano letters.* **2009**, vol. 9(1), p. 30 – 35 [cit. 2021-5-18]. ISSN 1530-6984. Available from: doi:10.1021/nl801827v.

[7] NOVOSELOV, K. S., GEIM A. K., MOROZOV, S. V., et al. Electric Field Effect in Atomically Thin Carbon Films. *Science,* vol. 306, p. 666 **2004**,[cit. 2021-5-17]. Available from: doi:10.1126/science.1102896.

[8] ŠTRBA, L. *Grafenový senzor relativní vlhkosti a vliv hradlového napětí.* Vysoké učení technické v Brně. Fakulta strojního inženýrství, **2018**.

[9] MAFRA, L. D. *Using inelastic scattering of light to understand the nature of electron-phonon interactions and phonon self-energy renormalizations in graphene materials.* Massachusetts Institute of Technology. Cambridge, MA, **2012**.

[10] Nanoscience *Atomic Force Microscopy.* [Online], [cit. 2021-5-18], available from: https://www.nanoscience.com/techniques/atomic-force-microscopy/.

[11] Maxiv *AFM scanning modes.* [Online], [cit. 2021-5-18], available from: https://www.maxiv.lu.se/accelerators-beamlines/support-labs-microscopy/atomic-force-microscopy/afm-scanning-modes/.

[12] BRYANT, P. J., MILLER, R. G., YANG, R. Scanning tunneling and atomic force microscopy combined. *Applied Physics Letters*, **1988**, Vol: 52 (26), p. 2233–2235, ISSN 0003-6951.

[13] CHUNG, K. and KIM, D. Wear characteristics of diamond-coated atomic force microscope probe. *Ultramicroscopy* Elsevier B.V, **2007**, vol. 108(1), p. 1–10 [cit. 2021-5-17]. ISSN 0304-3991. Available from: doi:10.1016/j.ultramic.2007.01.016.

[14] K-TEK Nanotechnology *NSG10/Au.* [Online], [cit. 2021-5-18], available from: https://kteknano.com/product/nsg10-au/.

[15] Nanosurf *Contact mode.* [Online], [cit. 2021-5-18], available from: https://www.nanosurf.com/en/support/afm-modes-overview/contact-modes.

[16] NT-MDT *Constant Height mode.* [Online], [cit. 2021-5-18], available from: https://www.ntmdt-si.com/resources/spm-principles/atomic-force-microscopy/contact-afm/constant-height-mode.

[17] NT-MDT *Non-contact mode.* [Online], [cit. 2021-5-18], available from: https://www.ntmdt-si.com/resources/spm-principles/atomic-force-microscopy/amplitude-modulation-afm/non-contact-mode.

[18] Park Systems *True Non-Contact Mode.* [Online], [cit. 2021-5-17], available from: https://parksystems.com/park-spm-modes/91-standard-imaging-mode/217-true-non-contact-mode.

[19] Science Direct *Tapping mode.* [Online], [cit. 2021-5-18], available from: https://www.sciencedirect.com/topics/engineering/tapping-mode.

[20] Nanosurf *Kelvin probe force microscopy (KPFM).* [Online], [cit. 2021-5-18], available from: https://www.nanosurf.com/en/support/afm-modes-overview/kelvin-probe-force-microscopy-kpfm.

[21] KUN, P., FÜLÖP, B., DOBRIK, G., et al. Robust quantum point contact operation of narrow graphene constrictions patterned by AFM cleavage lithography. *NPJ 2D materials and applications.* Nature Publishing Group, **2020**, vol. 4(1), p. 1–6 [cit. 2021-5-18]. Available from: doi:10.1038/s41699-020-00177-x.

[22] LU, G., ZHOU, X., LI, H., et al. Nanolithography of single-layer graphene oxide films by atomic force microscopy. *Langmuir: the ACS journal of surfaces and colloids.* **2010**, vol. 26(9), p. 6164 – 6166 [cit. 2021-5-18]. ISSN 07437463. Available from: doi:10.1021/la101077t.

[23] KONEČNÝ, M., BARTOŠÍK, M., MACH, J., et al. Kelvin Probe Force Microscopy and Calculation of Charge Transport in a Graphene/Silicon Dioxide System at Different Relative Humidity. *ACS applied materials and interfaces.* **2018**, vol. 10(14), p. 11987 – 11994 [cit. 2021-5-18]. ISSN 19448244. Available from: doi:10.1021/acsami.7b18041.

[24] TRIPSKÝ, A. *Studium šíření elektrického náboje na izolujícím povrchu pomocí Kelvinovy sondové mikroskopie při různých relativních vlhkostech.* Vysoké učení technické v Brně. Fakulta strojního inženýrství, **2018**.

Abbreviations

AFM   Atomic Force Microscope

KPFM   Kelvin Probe Force Microscopy

RH   Relative Humidity

PMMA   Poly(methyl methacrylate)

CVD   Chemical Vapor Deposition

BZ   Brillouin Zone

HOPG   Highly Oriented Pyrolytic Graphite

DCP   Diamond Coated Probe

LAO   Local Anodic Oxidation

RIE   Reactive Ion Etching

IPA   Isopropyl Alcohol

AC   Alternating Current

DC   Direct Current

A   Used AFM probes

	Diamond coated probe	Gold coated probe
Manufacturer	NT-MDT	AppNano
Model	DCP20	AN-NSG10/Au/50
Cantilever length (μm)	90	95
Cantilever width (μm)	60	30
Cantilever thickness (μm)	$1.7-2.3$	2
Resonant frequency (kHz)	$260-630$	250
Force constant (N/m)	$28-91$	11
Tip radius (nm)	$50-70$	<10
Tip height (μm)	$10-15$	$14-16$
Coat on reflective side	Gold (Au)	Gold (Au)
Coat on tip side	Diamond (thickness 70 nm)	Gold (Au)